# Utilising embeddings for maps of winter wheat and crop rotation in Henan China during 2018-2024

Ziwei Du[1], Keyi Rao[1], Chang Wu [1], Kexin Wang[1], Shixin Dong [1], Zhaocong Wu[1,2,*]

[1]School of Remote Sensing and Information Engineering, Wuhan University, China,
[2]Aerospace Information Research Institute, Henan Academy of Sciences, Henan 450046, China

**Keywords:** Winter wheat mapping, Rotation patterns, AlphaEarth Foundations, Satellite embedding dataset, Lightweight decoder.

**Abstract**

Accurate large-scale monitoring of wheat cultivation and its crop rotation patterns is essential for food security and agricultural management. However, traditional remote sensing classification approaches typically rely on long-term multi-source imagery, complex feature engineering, and extensive labelled samples, limiting their scalability and spatiotemporal generalisation. To address these challenges, this study explores the potential of the AlphaEarth Foundation (AEF) embeddings—a global, annual, analysis-ready satellite embedding dataset—for winter wheat and crop rotation mapping. Firstly, we analyze AEF embeddings for intra-class consistency and inter-class separability, assessing their effectiveness in representing wheat. Subsequently, we compare multiple lightweight classifiers to identify an optimal model and conduct spatiotemporal generalization experiments across Henan Province from 2018 to 2024 using only limited labelled samples from 2020. Based on the resulting wheat maps, crop rotation patterns are further identified. Experimental results demonstrate that AEF embeddings exhibit strong semantic coherence and discriminative capability. Acceptable accuracy (OA=0.85) can already be achieved with simple models like cosine similarity and linear regression. More advanced lightweight classifiers further improve performance (OA=0.86–0.93) while maintaining stable results across different years and regions (spatial consistency=0.82). In addition, the crop rotation maps show high spatial agreement with existing products, while producing more spatially contiguous field patterns. Overall, AEF embeddings can serve as effective, ready-to-use features for large-scale agricultural remote sensing applications. By substantially reducing reliance on complex feature engineering and extensive training samples, they provide a practical and scalable solution for mapping winter wheat and its crop rotation patterns.

## 1. INTRODUCTION

Accurate crop mapping is essential for agricultural monitoring, food security assessment, and policy-making under increasing environmental pressure and the growing demand for sustainable agricultural production (Wu et al., 2023). However, remote sensing-based crop mapping still faces two persistent challenges: the scarcity of labelled samples and the difficulty of effectively integrating multi-source observations. Recently, AlphaEarth Foundations (AEF) (Brown et al., 2025) has provided a new opportunity to address these challenges. As a large-scale Earth observation foundation model, AEF integrates optical, radar, and LiDAR data at petabyte scale to generate a unified 64-dimensional representation of the Earth's surface (Brown et al., 2025). Such embedding-based representations may reduce dependence on task-specific feature engineering and improve downstream performance under limited training data (Wang et al., 2026, Jin et al., 2026). Therefore, it is important to evaluate whether they are suitable for crop mapping for advancing large-scale monitoring.

Winter wheat is one of the most important staple crops in China and worldwide, playing a critical role in food security and agricultural policy-making (Dong et al., 2024). Its spatial distribution and planting structure are closely related to regional agricultural systems (Li et al., 2022). Moreover, winter wheat is a suitable target for testing embedding-based representations because its identification typically relies on multi-temporal and multi-source information, while its phenological characteristics vary across years and regions. The AEF embedding dataset released on Google Earth Engine (GEE) provides a standardized feature basis for crop identification and crop rotation analysis, offering the potential to support more transferable classification across space and time.

Existing crop mapping methods can generally be divided into knowledge-driven and data-driven approaches (Fang et al., 2024, Mahlayeye et al., 2022). Knowledge-driven approaches usually construct classification rules based on vegetation index trajectories or carefully designed spectral indicators (Qiu et al., 2017, Qu et al., 2021, Yang et al., 2023b). These methods are often interpretable, but they depend heavily on prior knowledge and empirical thresholds, which limits their adaptability to regional differences and interannual phenological variation (Zeng et al., 2020, Wu et al., 2023). In contrast, data-driven approaches, including random forests and deep learning models, improve classification accuracy through multi-source feature fusion (Li et al., 2022, Yue et al., 2025), and have also enabled automated sample generation (Gao et al., 2023) and cross-year transfer frameworks (Hu et al., 2022). Nevertheless, such approaches typically require large amounts of annotated data and may suffer from overfitting or reduced generalization in data-scarce, cross-regional, or cross-temporal scenarios (Teixeira et al., 2023, Qi et al., 2024). These limitations indicate the need for a representation framework that can capture rich spatiotemporal information while reducing dependence on extensive labelled samples and handcrafted features.

Brown et al. showed that AEF embeddings can substantially improve downstream task performance under low-data conditions (Brown et al., 2025). However, it is still unclear whether AEF embeddings provide adequate intra-class consistency and inter-class separability for agricultural categories, and whether they can support robust spatiotemporal transfer under small-

sample conditions. A systematic evaluation of AEF embeddings in these contexts is therefore needed.

To address these gaps, this study investigates the feasibility and generalization capability of AEF embeddings for winter wheat and wheat rotation classification under limited-sample conditions. The objectives of this study are as follows: (1) to evaluate the intra-class consistency and inter-class separability of AEF embeddings for winter wheat classification tasks; (2) to map winter wheat in Henan Province from 2018 to 2024 and evaluate the spatiotemporal transferability and classification accuracy of the model; and (3) to examine whether the same embedding representation can be extended from winter wheat mapping to wheat rotation classification.

## 2. MATERIALS AND METHODS

### 2.1 Study area and samples

This study evaluates the potential of the AEF embedding dataset for mapping winter wheat and associated rotation patterns in Henan Province, China, a major agricultural region that contributes approximately 28% of the national wheat production (Sheng et al., 2025). Located at 31.22°–36.22°N and 110.21°–116.39°E, Henan is characterized by a dominant double-cropping system, in which winter wheat is typically followed by summer crops such as maize, soybean, or rice (Yang et al., 2023a). We classify the winter wheat and further explore the patterns of its rotation systems across the province. Annual AEF embeddings from 2018 to 2024 were accessed in Google Earth Engine, and the overall workflow is shown in Figure 1.

Reference samples for winter wheat mapping were derived from in-situ point observations collected during field surveys conducted in May 2024 in Hebi City. Using a spatially balanced sampling strategy, 345 points were selected and labelled as non-wheat (0) or winter wheat (1). These samples were randomly divided into training (70%) and validation (30%) subsets.

Reference samples for rotation mapping were generated through visual interpretation of PlanetScope monthly composite imagery (Team, 2017), guided by the ChinaCP-Wheat10m dataset (Qiu et al., 2025). A systematic grid-based sampling approach generated 270 sample points (0: background, 1-3: rotation classes), subsequently divided into 70% for training and 30% for validation.

### 2.2 Method framework

We first assessed the representation characteristics of AEF embeddings for winter wheat classification in terms of intra-class consistency and inter-class separability. Feature vectors were extracted from wheat and non-wheat samples. Class-wise feature means and variances were computed to characterize class centers and intra-class dispersion. Class centroids were then derived, and the cosine similarity between each sample and its corresponding centroid was calculated to evaluate within-class consistency in the embedding space. In addition, principal component analysis (PCA) was applied to project the embeddings into two dimensions for visual inspection of clustering patterns.

To evaluate the effectiveness of the AEF embedding, seven lightweight classifiers available in the built-in GEE library (Gorelick et al., 2017) were implemented, including Random Forest (RF), K-Nearest Neighbours (KNN), Support Vector Machine with linear and radial basis function kernels (SVM_LINEAR and SVM_RBF), Classification and Regression Trees (CART), Naive Bayes (NB), and Gradient Boosting Trees (GBT). Model hyperparameters were tuned using grid search with five-fold cross-validation, and the best-performing classifier was selected based on validation performance.

For comparison with a conventional baseline, we constructed a handcrafted feature-engineering baseline using Sentinel-2 imagery. Images acquired during the winter wheat growing season (from October of the preceding year to June of the target year) were cloud-masked using the Scene Classification Layer and composited into monthly median images. Based on these composites, four vegetation indices reflecting seasonal growth dynamics (NDVI, EVI, NDRE, and LSWI) and their derived temporal features were extracted. Specifically, temporal features were extracted from key growth stages of winter wheat. For example, NDVI-based features captured overwintering (December–January) and peak-season (April–May) dynamics, and sampled during spring or heading stages to reflect leaf chlorophyll content, water status, or canopy development. Overall, these calculations produced a 46-dimensional feature vector, which was used as input to the same classifier with the same training samples and parameter settings as in the embedding-based experiments.

To assess the spatiotemporal generalization capacity, the optimal model was trained and applied to classify winter wheat across the entire province of Henan from 2018 to 2024. This experiment simulated a practical “cross-year and cross-region classification without relabeling” scenario. Classification results were used to estimate area at both provincial and municipal scales to evaluate the consistency and robustness of area estimation across spatiotemporal domains.

We further explored the potential of embeddings in more complex land cover semantic discrimination by training a model on wheat rotation samples from Henan to classify three rotation patterns: wheat–maize, wheat–rice, and wheat–others (including other double-season crops or single-season wheat). This task requires recognizing both the temporal signatures of winter wheat and subsequent crops, representing a more refined semantic classification scenario, and helps verify the sensitivity of embeddings to growth stages and cropping systems.

Classification performance was evaluated using four standard metrics, including Overall Accuracy (OA), F1 Score, User’s Accuracy (UA), and Producer’s Accuracy (PA). For area estimation, we applied the area-weighted confusion matrix method (Olofsson et al., 2014) to mitigate class imbalance and generate reliable estimates with uncertainty intervals. Municipal-level estimates were then compared against statistical data to assess the model’s practical applicability.

## 3. RESULTS AND DISCUSSION

### 3.1 Feature representation capability of AEF embeddings

Analysis of the embedding vectors reveals distinct distributional characteristics. Wheat samples exhibit high internal consistency, with a compact distribution (mean variance = 0.012), indicating that the embeddings reliably capture coherent features of winter wheat. After applying PCA to the embedding vectors, the resulting 2D feature distribution shows clear clustering of wheat samples, whereas non-wheat samples remain scattered (Figure 2b), showing the inherent separability of AEF embeddings for wheat identification.

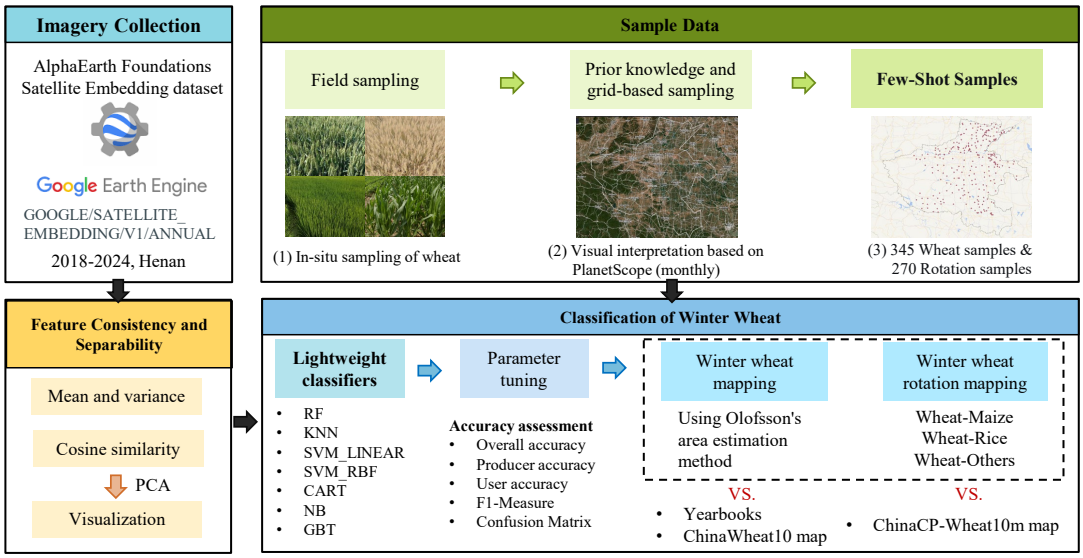


Figure 1. The flowchart of the study.

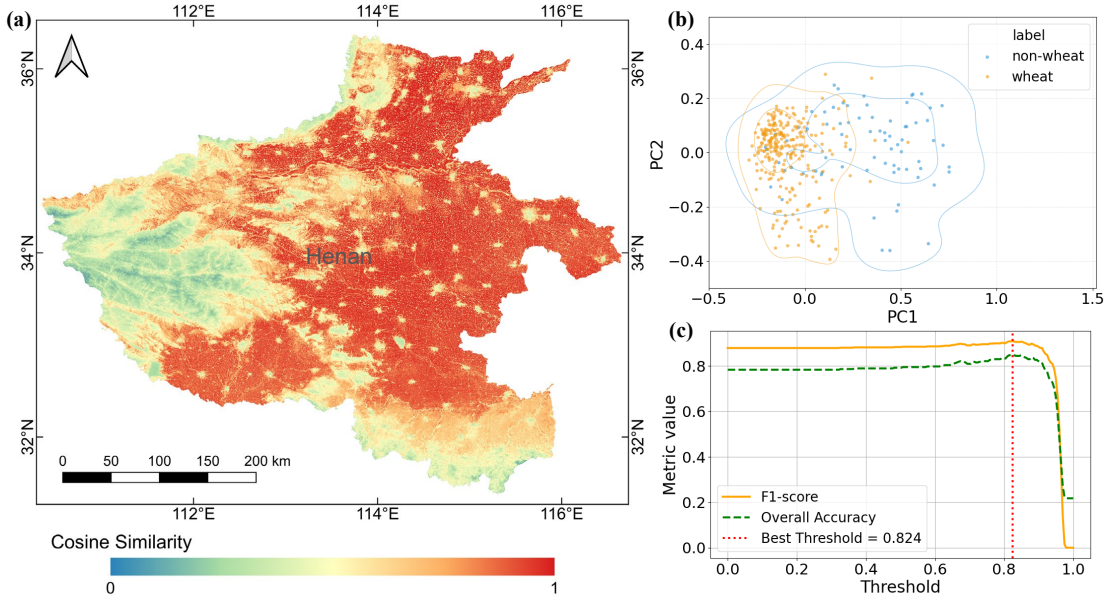


Figure 2. Assessment of feature consistency and separability. (a) Similarity map based on cosine. (b) PCA of embeddings. (c) Threshold optimization.

A binary classification approach further quantified this separability. Using the mean wheat vector as a feature centroid, cosine similarity values were computed for all pixels to generate a similarity map (Figure 2a). Linear regression analysis determined an optimal classification threshold of 0.824 (Figure 2c), achieving a sample-level F1 score of 0.908 and OA of 0.849. These results demonstrate that satisfactory classification accuracy can be achieved without further feature engineering, confirming the strong discriminative capacity and semantic expressiveness of AEF embeddings in characterizing wheat cultivation areas.

AEF embedded datasets establish a more effective paradigm for remote sensing classification by shifting from feature engineering to semantic representations. While conventional approaches depend on manually designed features (Mehmood et al., 2022), such as NDVI, EVI, that exhibit limited generalizability (Qiu et al., 2017), AEF embeddings serve as a ready-to-use input that inherently encodes discriminative information sufficient for accurate crop classification. This is validated by our results, where a simple linear model achieved an OA of 0.849. This ability stems from several key advantages: inherent spatiotemporal consistency, elimination of manual feature engineering, and immediate usability for rapid, large-scale mapping. These pre-trained features provide a powerful basis for advanced applications such as cross-regional transfer learning and fine-scale crop rotation analysis.

### 3.2 Classifier performance on AEF embeddings

We systematically tuned hyperparameters for seven classifiers in GEE, with the optimal parameters sets summarized in Table 1. All classifiers achieve high accuracy using AEF embeddings, with OA exceeding 85% across all models (Table 1), indicating strong feature separability and robustness. Among them, RF

This contribution has been peer-reviewed. The double-blind peer-review was conducted on the basis of the full paper.
https://doi.org/10.5194/isprs-annals-XI-2-2026-865-2026 | © Author(s) 2026. CC BY 4.0 License.

Table 1. Performance comparison of AEF embeddings and the RS baseline

| Model | Optimal parameters | AEF embeddings / RS baseline | | | |
|---|---|---|---|---|---|
| | | OA | F1 | Mean PA | Mean UA |
| RF | max_depth=20, min_samples_split=2, n_estimators=200 | **0.933** / 0.922 | 0.930 / **0.951** | 0.863 / 0.851 | 0.937 / 0.909 |
| KNN | n_neighbors=5 | 0.931 / 0.912 | 0.928 / 0.905 | 0.848 / 0.812 | **0.960** / 0.921 |
| SVM_RBF | C=10, $\gamma$=0.1 | 0.913 / 0.922 | 0.907 / 0.923 | 0.820 / **0.901** | 0.923 / 0.877 |
| SVM_LINEAR | C=10 | 0.923 / 0.931 | 0.919 / 0.931 | 0.842 / 0.890 | 0.930 / 0.904 |
| CART | max_depth=None, min_samples_split=2 | 0.875 / 0.902 | 0.874 / 0.903 | 0.817 / 0.872 | 0.839 / 0.849 |
| NB | default settings | 0.856 / 0.902 | 0.861 / 0.905 | 0.830 / 0.888 | 0.789 / 0.846 |
| GBT | learning_rate=0.05, max_depth=5, n_estimators=100, subsample=0.7 | **0.933** / 0.892 | 0.930 / 0.891 | 0.863 / 0.832 | 0.937 / 0.844 |

and GBT performed best, achieving an average OA of 0.933 and an F1 score of 0.930, with UA and PA of 0.937 and 0.863, respectively. KNN ranked next (OA = 0.931, F1 = 0.928), followed by SVM_LINEAR and SVM_RBF, both exceeding 0.9 OA, confirming their ability to capture complex nonlinear patterns in the high-dimensional embedding space. CART and NB showed slightly lower performance (OA = 0.875 and 0.856), but remained reasonably accurate ($> 0.85$). For comparison, the traditional remote sensing baseline based on 46 handcrafted spectral and index-derived features achieves comparable accuracy. Despite the similar accuracy, constructing the baseline requires dense, cloud-free time-series imagery from December to June and extensive feature engineering. In contrast, AEF embeddings provide a compact, analysis-ready representation while maintaining comparable classification performance.

The high and stable classification accuracy of AEF embeddings across multiple models (mean OA $> 0.9$) indicates low sensitivity to classifier type. This model-agnostic property points to a well-structured feature space capable of delivering stable predictions. Considering classification accuracy, computational efficiency, and cross-spatial generalisation capability, the RF model was selected as the final classifier for wheat identification due to its high performance, low computational cost, and robustness to overfitting.

### 3.3 Spatiotemporal generalization capacity

The proposed classifier demonstrates strong spatiotemporal generalization capability across multiple years and diverse topographic regions in Henan Province. For the 2020 winter wheat classification, we systematically compare our results with two existing products: ChinaWheat10 (Yang et al., 2023b) and the TWDTW-based map (Dong et al., 2020). Qualitative assessment indicates strong spatial agreement between our classification and both reference products in identifying winter wheat extents (Figure 4). Visually, our results achieve higher internal parcel homogeneity and effectively reduce misclassification along field boundaries and non-crop features. Quantitatively, using randomly sampled points from the high-accuracy ChinaWheat10 map (F1=0.94) for validation, our model achieves an overall accuracy of 0.8157. Then, the 2020 wheat area after good practice for area estimation across 18 cities shows a strong fit with official census data (Figure 3b). The regression equation is $y = 0.99x - 355.22$, with an $R^2 = 0.988$ and $p < 0.01$, indicating high consistency between the model-derived area and statistical data. This agreement underscores the strong spatiotemporal transferability of AEF embeddings across years and regions, as well as their robustness to variations in radiometric, meteorological, and observational conditions.

Furthermore, we generated winter wheat distribution maps for the consecutive seven-year period from 2018 to 2024. The resulting cultivation frequency map (Figure 3a) accurately reflects the spatiotemporal patterns of winter wheat in Henan Province. The maps show that winter wheat is predominantly concentrated in the central-eastern and northern plains, forming contiguous high-frequency cultivation zones. In contrast, cultivation in the southern and western hilly and mountainous regions is fragmented and sparse due to terrain constraints and landscape heterogeneity. This spatial distribution consistent with established agricultural zonation and major wheat-producing areas, further validating the practical plausibility of our classification results. In terms of area dynamics, the estimated annual wheat area shows certain interannual fluctuations (Figure 3c). Although the general trend from 2018 to 2023 aligns with Statistics yearbook data, the classified results consistently underestimate the area by about 8%–20%. This discrepancy may be attributable to the omission of fragmented plots, sloping cultivated land, and scattered cultivation in mountainous areas, as analysed in Section 3.4. Despite this systematic underestimation, the classified data effectively capture interannual variation trends, confirming the temporal stability and reliability of the classification system.

The results demonstrate that the model based on AEF embeddings effectively generalizes across temporal and spatial domains. A model trained solely on 2024 samples from Hebi City maintained stable performance when directly applied to provincial-scale data from 2018-2024 (OA = 0.8157, F1 = 0.802 for 2020). This spatio-temporal transferability can mitigate a challenge in agricultural remote sensing, winter wheat's distinct seasonal growth patterns and regional variations often cause models trained in specific spatio-temporal domains to degrade under different conditions (Hoppe et al., 2024).

The transferability stems from AEF embedding fundamental architecture. Unlike traditional approaches dependent on manually designed temporal features or region-specific training data, AEF embeddings are constructed from global multi-temporal, multi-sensor imagery across diverse ecological zones (Brown et al., 2025). This enables similar crop types to maintain consistent semantic representations across different years, climates, and sensing conditions, capturing both temporal dynamics and invariant high-level semantics. The strong agreement in area estimation between our results and official statistics ($R^2 = 0.988, p < 0.01$) further substantiates the robustness of

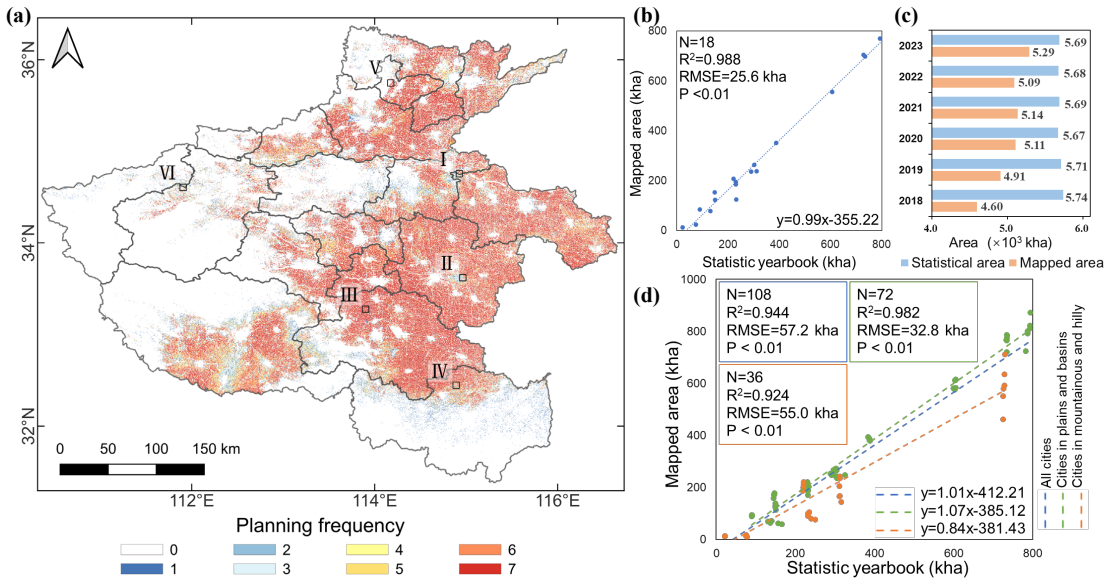


Figure 3. Classification of Winter Wheat in Henan. (a) Winter wheat cultivation frequency (2018-2024, Henan). (b) Henan municipal comparison with Statistical Yearbooks (2020). (c) Henan provincial comparison with Statistical Yearbooks (2018-2023). (d) Comparison with Statistical Yearbooks of different terrains (2018-2023)

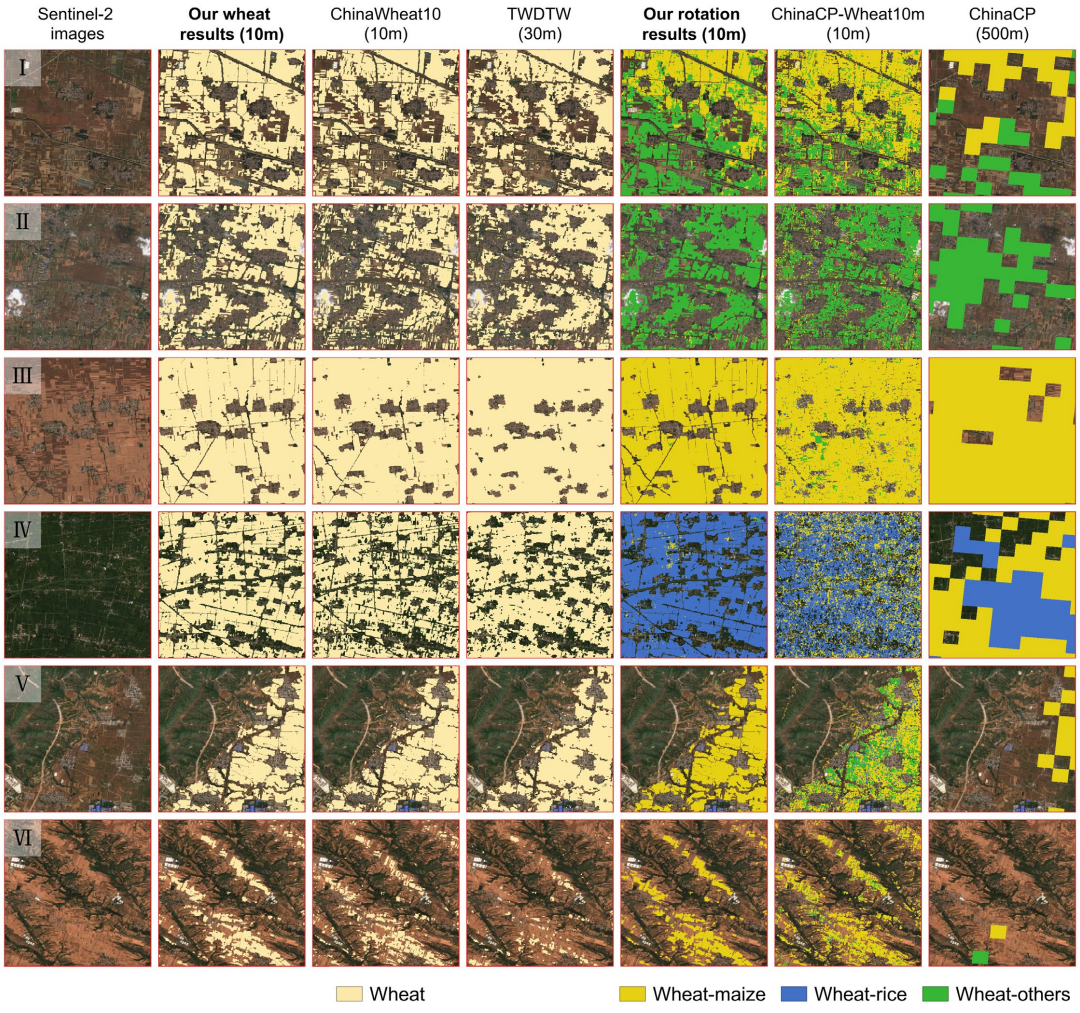


Figure 4. Spatial distribution and typical region comparison map of winter wheat and its rotation in 2020. The location of typical regions (I-VI) was marked in Figure 3a.

embeddings to radiometric, meteorological, and observational inconsistencies.

This spatiotemporal transferability has practical implications. First, it reduces reliance on high-quality annotated samples, overcoming the bottleneck in traditional methods that require repeated sample collection and feature re-engineering (Antonijević et al., 2023). Second, it improves automation and timeliness for annual, large-scale crop monitoring. Third, the stable cross-region performance confirms that embeddings provide a universal feature space where crop types maintain consistent representations across geographical settings (Brown et al., 2025). This study confirms the strong transferability and spatiotemporal generalization capacity of AEF embeddings in winter wheat classification. Accurate crop identification and area estimation can be achieved without complex feature engineering or annual retraining.

### 3.4 Topographic influences and limitations

To evaluate the robustness of embedding features under complex terrain, Henan was divided into two topographic zones based on geomorphological characteristics: (1) Plains and Basins (northern, eastern, and central areas, 55.7% of total area), and (2) Mountainous and Hilly Regions (44.3%) (Li et al., 2015). Overall, the classified winter wheat area showed strong agreement with statistical data across 2018–2023 ($\mathrm{y} = 1.01\mathrm{x} - 412.21$, with $\mathrm{R}^2 = 0.944$; Figure 3d), demonstrating that embeddings maintain semantic consistency and generalisation stability across varied terrain.

In plains and basins, winter wheat fields show clear boundaries and structural integrity. The model effectively captured cropland texture and phenological variation, achieving an excellent municipal-level fit ($y = 1.07x - 385.12$, $R^2 = 0.982$). Stable illumination, uniform reflectance, and large-scale cultivation patterns in these areas facilitated the formation of consistent ”crop clusters” in the semantic space (Wang et al., 2023), minimizing feature aliasing. This advantage stems from the more stable temporal-spectral characteristics of winter wheat in flat terrain, where embeddings can better represent spatiotemporal continuity and growth dynamics compared to traditional methods.

In contrast, mountainous and hilly areas showed reduced performance ($y = 0.84x - 381.43$ and $R^2 = 0.924$), with noticeable area underestimation. This decline reflects challenges in complex terrain: topographic occlusion, slope effects, and fragmented land use disperse wheat plots and cause spectral mixing with non-crop features (Xu et al., 2024). Spectral-temporal signatures in these regions are frequently disrupted by terrain shadows, soil background effects, and mixed vegetation signals, reducing feature separability in the embedding space. Furthermore, significant topographic variation strongly influences cropping patterns through microclimate effects, slope constraints, and elevation gradients (Liang et al., 2024).

These performance variations reveal limitations of current embeddings. Although AEF embeddings maintain competent high-level semantic representation, complex topography persistent challenges—including shadow effects, geometric distortion in optical imagery, and localized SAR signal interference (Imperatore, 2021). Moreover, landscape fragmentation in mountainous areas undermines the continuity assumptions inherent in patch-based semantic modeling (Liu et al., 2025). This suggests that future crop classification studies—whether global or regional—should more explicitly account for topographic influences on remote sensing features. Developing embedding adaptation and transfer learning strategies tailored to different ecological zones will be essential to improve model robustness and universality across diverse landscapes.

### 3.5 Identification of wheat rotation patterns

Building on the optimized random forest model integrated with embedding features, we generated the typical spatial distribution of winter wheat rotation patterns across Henan for 2020. Results show that wheat-maize rotation dominates the provincial cropping system, occupying approximately 72.8% of wheat-growing areas. This pattern is most concentrated in the central and northern plains, forming contiguous zones in places like Xinxiang and Anyang, where flat terrain, reliable irrigation, and developed infrastructure support intensive grain production. In contrast, wheat-rice rotation is primarily distributed south of the Huai River—particularly in northern Xinyang—with minor clusters in southern Xinxiang, northern Kaifeng, and southeastern Puyang, accounting for only 5.0% of the total area. The wheat–other pattern constitutes approximately 22.2% of the area, including rotations with soybean, peanut, sesame, or cotton, as well as single-season wheat.

We conducted a comparative analysis against two established products (Figure 4): ChinaCP-Wheat10m (Qiu et al., 2025) and ChinaCP (Qiu et al., 2022). The resolution of ChinaCP is relatively low, and it is difficult to identify the detailed location of the winter wheat and its rotation patterns. Comparison with the ChinaCP-Wheat10m dataset demonstrates strong spatial agreement at both macro and micro scales, while our embedding-based results exhibit clearer field boundaries and better within-field continuity. At the macro-spatial level, both datasets consistently reflect the dominant wheat-maize rotation in central-northern plains, wheat-rice south of the Huai River, and scattered wheat–other patterns in hilly transition zones and peri-urban areas. This spatial structure aligns with known agricultural systems and climatic gradients, confirming the reliability of embedding features in capturing rotation-type differentiation. At the local scale, our classification shows improved performance (Figure 4), field boundaries appear smoother, with similar pixels exhibiting stronger aggregation, indicating enhanced internal parcel-level consistency and improved spatial continuity. Furthermore, micro-regional analysis shows that our results better maintain categorical continuity within fields while reducing salt-and-pepper noise, particularly evident in the southern wheat-rice zone.

The successful identification of winter wheat rotation patterns represents a significant advancement over existing approaches, which have predominantly focused on discriminating individual crop types rather than integrated cropping sequences (Li et al., 2023). Typical rotation systems—such as winter wheat–summer maize and winter wheat–summer rice—exhibit unique spectral-phenological signatures during crop successions, leading conventional methods to rely heavily on manually constructed multi-temporal features, time-series indices, or land use records (Qiu et al., 2025). In contrast, the core strength of AEF embeddings lies in their capacity to autonomously learn semantic continuity across spatiotemporal scales through large-scale remote sensing modeling. While traditional approaches require explicit design of temporal feature sets, AEF embeddings automatically encode cross-seasonal growth rhythms directly within the feature space, achieving

effective clustering and separation of different rotation types without manual feature engineering.

The consistent performance of embeddings across years and regions reflects their strong generalization capacity within agricultural systems. Pre-trained on global crop growth patterns and environmental contexts, the model captures stable seasonal and rotational cycles, supporting both single-year static monitoring and multi-year dynamic mapping. For example, transferring the model to time-series data from Henan and Shandong allows continuous tracking of winter wheat rotation systems from 2018 to 2025, revealing regional shifts in cropping structure. The same framework can be extended to other crop systems, such as rice–rapeseed or maize–peanut, enabling scalable and transferable rotation mapping.

From an application standpoint, the rotation identification capability of AEF embeddings offers agricultural authorities a powerful analytical tool. Integration with land use databases, meteorological data, and water resource information enables regional assessment of the ecological benefits and production risks associated with different rotation systems. In regions like the Huang-Huai-Hai Plain, where the winter wheat–summer maize system dominates but faces sustainability challenges due to water scarcity and climate change, dynamic rotation monitoring can identify high water-consumption areas, cropping intensity hotspots, and policy-induced transitions, supporting data-driven agricultural planning. Looking forward, this study opens avenues for constructing a unified ”crop rotation semantic space.” Future work may incorporate temporal Transformers or causal inference modules to explicitly represent crop succession mechanisms, moving toward a more interpretable ”crop life cycle characterization.”

## 4. Conclusion

This study systematically evaluates the application potential of the AEF embedding dataset for winter wheat identification and crop rotation pattern interpretation. Results confirm its effectiveness and transferability as a general-purpose remote sensing feature for crop classification tasks. Without the need for complex feature engineering, AEF embeddings effectively capture the spectral and temporal semantics of winter wheat (the average OA across seven classifiers exceeds 0.9, comparable to the accuracy of the RS baseline with 46 features), showing strong feature consistency, separability, and notable spatiotemporal generalization capability (spatial consistency with validation data was 0.815, while the $R^2$ value for statistical data fitting in 2020 was 0.988). In identifying rotation patterns, the embeddings align spatially with existing high-precision maps while offering improved detail resolution, highlighting their ability to discern crop transition semantics and demonstrating substantial practical relevance.

This work shows that AEF embeddings serve as a ready-to-use feature enabling high-precision crop classification and rotation interpretation without complex modeling. Their strong generalizability and semantic expressiveness support a shift in agricultural remote sensing from manual feature design toward intelligent mapping based on deep semantic representation. Future work will further validate the spatiotemporal generalizability of AEF embeddings across diverse cropping systems and establish a multi-annual, multi-crop dynamic monitoring framework for rotation patterns. We also plan to extend evaluation to other staple crops toward a unified, cross-regional crop mapping paradigm. These efforts are expected to promote the broader adoption of intelligent remote sensing features in global agricultural monitoring and sustainable cropland management.

## Acknowledgements

This project is supported by the Startup Research Fund of Henan Academy of Sciences (No.242025005), China; and the Joint Fund of Henan Province Science and Technology R&D Program (No.235200810001), China. The numerical calculations in this paper have been done on the supercomputing system in the Supercomputing Center of Wuhan University.

## References

Antonijević, M., Petrović, V., Ćirić, I., Milivojević, D., Milivojević, Z., 2023. Transfer learning approach based on satellite image time series for the crop classification problem. *Journal of Big Data*, 10(1), 107.

Brown, C. F., Kazmierski, M. R., Pasquarella, V. J., Rucklidge, W. J., Samsikova, M., Zhang, C., Shelhamer, E., Lahera, E., Wiles, O., Ilyushchenko, S. et al., 2025. Alphaearth foundations: An embedding field model for accurate and efficient global mapping from sparse label data. *arXiv preprint arXiv:2507.22291*.

Dong, J., Fu, Y., Wang, J., Tian, H., Fu, S., Niu, Z., Han, W., Zheng, Y., Huang, J., Yuan, W., 2020. Early season mapping of winter wheat in China based on Landsat and Sentinel images. *Earth System Science Data Discussions*, 2020, 1–26.

Dong, J., Pang, Z., Fu, Y., Peng, Q., Li, X., Yuan, W., 2024. Annual winter wheat mapping dataset in China from 2001 to 2020. *Scientific Data*, 11(1), 1218.

Fang, H., Liang, S., Chen, Y., Ma, H., Li, W., He, T., Tian, F., Zhang, F., 2024. A comprehensive review of rice mapping from satellite data: Algorithms, product characteristics and consistency assessment. *Science of remote sensing*, 10, 100172.

Gao, Y., Pan, Y., Zhu, X., Li, L., Ren, S., Zhao, C., Zheng, X., 2023. FARM: A fully automated rice mapping framework combining Sentinel-1 SAR and Sentinel-2 multi-temporal imagery. *Computers and Electronics in Agriculture*, 213, 108262.

Gorelick, N., Hancher, M., Dixon, M., Ilyushchenko, S., Thau, D., Moore, R., 2017. Google Earth Engine: Planetary-scale geospatial analysis for everyone. *Remote Sensing of Environment*, 202, 18-27. https://www.sciencedirect.com/science/article/pii/S0034425717302900. Big Remotely Sensed Data: tools, applications and experiences.

Hoppe, H., Dietrich, P., Marzahn, P., Weiß, T., Nitzsche, C., Freiherr von Lukas, U., Wengerek, T., Borg, E., 2024. Transferability of Machine Learning Models for Crop Classification in Remote Sensing Imagery Using a New Test Methodology: A Study on Phenological, Temporal, and Spatial Influences. *Remote Sensing*, 16(9), 1493.

Hu, Y., Zeng, H., Tian, F., Zhang, M., Wu, B., Gilliams, S., Li, S., Li, Y., Lu, Y., Yang, H., 2022. An interannual transfer learning approach for crop classification in the Hetao Irrigation district, China. *Remote Sensing*, 14(5), 1208.

Imperatore, P., 2021. SAR Imaging Distortions Induced by Topography: A Compact Analytical Formulation for Radiometric Calibration. *Remote Sensing*, 13(16).

Jin, C., Jiang, X., Wen, L., Wu, C., Xu, X., Jiao, J., 2026. Assessing the Utility of Satellite Embedding Features for Biomass Prediction in Subtropical Forests with Machine Learning. *Remote Sensing*, 18(3). https://www.mdpi.com/2072-4292/18/3/436.

Li, C., Chen, W., Wang, Y., Wang, Y., Ma, C., Li, Y., Li, J., Zhai, W., 2022. Mapping winter wheat with optical and SAR images based on Google Earth Engine in Henan Province, China. *Remote Sensing*, 14(2), 284.

Li, H., Song, X.-P., Hansen, M. C., Becker-Reshef, I., Adusei, B., Pickering, J., Wang, L., Wang, L., Lin, Z., Zalles, V., Potapov, P., V. Stehman, S., Justice, C., 2023. Development of a 10-m resolution maize and soybean map over China: Matching satellite-based crop classification with sample-based area estimation. *Remote Sensing of Environment*, 294.

Li, J., Liu, Y., Cao, M., Xue, B., 2015. Space-time characteristics of vegetation cover and distribution: Case of the Henan Province in China. *Sustainability*, 7(9), 11967–11979.

Liang, T., Tian, F., Zou, L., Jin, H., Tagesson, T., Rumpf, S., He, T., Liang, S., Fensholt, R., 2024. Global assessment of vegetation patterns along topographic gradients. *International Journal of Digital Earth*, 17(1).

Liu, M., Wu, F., Mo, C., Xiao, R., Yu, H., Wang, M., 2025. Heterogeneous Changes and Evolutionary Characteristics of Cultivated Land Fragmentation in Mountainous Counties and Townships in Southwest China: A Case Study of Beichuan Qiang Autonomous County. *Land*, 14(7).

Mahlayeye, M., Darvishzadeh, R., Nelson, A., 2022. Cropping patterns of annual crops: A remote sensing review. *Remote Sensing*, 14(10), 2404.

Mehmood, M., Shahzad, A., Zafar, B., Shabbir, A., Ali, N., 2022. Remote sensing image classification: A comprehensive review and applications. *Mathematical problems in engineering*, 2022(1), 5880959.

Olofsson, P., Foody, G. M., Herold, M., Stehman, S. V., Woodcock, C. E., Wulder, M. A., 2014. Good practices for estimating area and assessing accuracy of land change. *Remote sensing of Environment*, 148, 42–57.

Qi, H., Qian, X., Shang, S., Wan, H., 2024. Multi-year mapping of cropping systems in regions with smallholder farms from Sentinel-2 images in Google Earth engine. *GIScience & Remote Sensing*, 61(1), 2309843.

Qiu, B., Hu, X., Chen, C., Tang, Z., Yang, P., Zhu, X., Yan, C., Jian, Z., 2022. Maps of cropping patterns in China during 2015–2021. *Scientific data*, 9(1), 479.

Qiu, B., Li, Z., Yang, P., Wu, W., Chen, X., Wu, B., Zhang, M., Duan, Y., Kurniawan, S., Tryjanowski, P. et al., 2025. Towards automation of national scale cropping pattern mapping by coupling Sentinel-1/2 data: A 10-m map of crop rotation systems for wheat in China. *Agricultural Systems*, 227, 104338.

Qiu, B., Luo, Y., Tang, Z., Chen, C., Lu, D., Huang, H., Chen, Y., Chen, N., Xu, W., 2017. Winter wheat mapping combining variations before and after estimated heading dates. *ISPRS journal of photogrammetry and remote sensing*, 123, 35–46.

Qu, C., Li, P., Zhang, C., 2021. A spectral index for winter wheat mapping using multi-temporal Landsat NDVI data of key growth stages. *ISPRS journal of photogrammetry and remote sensing*, 175, 431–447.

Sheng, K., Li, R., Zhang, F., Chen, T., Liu, P., Hu, Y., Li, B., Song, Z., 2025. Response of Grain Yield to Extreme Precipitation in Major Grain-Producing Areas of China Against the Background of Climate Change—A Case Study of Henan Province. *Water*, 17(15), 2342.

Team, P., 2017. Planet application program interface: In space for life on Earth. *Planet*.

Teixeira, I., Morais, R., Sousa, J. J., Cunha, A., 2023. Deep learning models for the classification of crops in aerial imagery: A review. *Agriculture*, 13(5), 965.

Wang, W., Guo, H., He, S., Qi, F., Samat, A., Wang, D., Li, J., 2026. AI-Driven Precision Mapping of Tea Plantations Using AlphaEarth Foundations: A Scalable Solution for Smart Agricultural Monitoring. *Agriculture*, 16(4). https://www.mdpi.com/2077-0472/16/4/412.

Wang, X., Liu, J., Peng, P., Chen, Y., He, S., Yang, K., 2023. Automatic Crop Classification Based on Optimized Spectral and Textural Indexes Considering Spatial Heterogeneity. *Remote Sensing*, 15(23), 5550.

Wu, B., Zhang, M., Zeng, H., Tian, F., Potgieter, A. B., Qin, X., Yan, N., Chang, S., Zhao, Y., Dong, Q. et al., 2023. Challenges and opportunities in remote sensing-based crop monitoring: A review. *National Science Review*, 10(4), nwac290.

Xu, X., Li, D., Liu, H., Zhao, G., Cui, B., Yi, Y., Yang, W., Du, J., 2024. Comparative Validation and Misclassification Diagnosis of 30-Meter Land Cover Datasets in China. *Remote Sensing*, 16(22).

Yang, B., Wang, J., Li, S., Huang, X., 2023a. Identifying the Spatio-Temporal Change in Winter Wheat–Summer Maize Planting Structure in the North China Plain between 2001 and 2020. *Agronomy*, 13(11), 2712.

Yang, G., Li, X., Liu, P., Yao, X., Zhu, Y., Cao, W., Cheng, T., 2023b. Automated in-season mapping of winter wheat in China with training data generation and model transfer. *ISPRS Journal of Photogrammetry and Remote Sensing*, 202, 422–438.

Yue, T., Fang, H., Ma, S., Wang, Q., Jiang, J., Song, B., Li, J., Chen, Y., Huang, H., 2025. Fine-grained classification of Orah mandarin tree plots in UAV remote sensing images based on GACL-DeepLabV3+. *Computers and Electronics in Agriculture*, 239, 110897.

Zeng, L., Wardlow, B. D., Xiang, D., Hu, S., Li, D., 2020. A review of vegetation phenological metrics extraction using time-series, multispectral satellite data. *Remote Sensing of Environment*, 237, 111511.